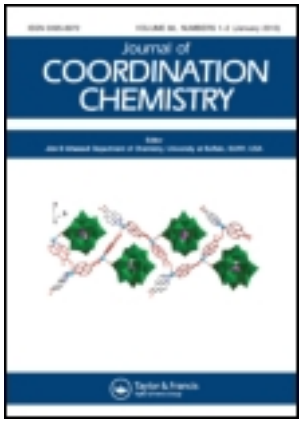

Journal of Coordination Chemistry
Publication details, including instructions for authors and subscription information:
http://www.tandfonline.com/loi/gcoo20

Study on interaction of N,N′-(2-hydroxy-3-methoxybenzyl) diamine cerium(IV) with bovine serum albumin

Hai-Tao Xia[a], Yu-Fen Liu[a] & Wei-Xing Ma[a]
[a] School of Chemical Engineering, Huaihai Institute of Technology, Lianyungang, China

Accepted author version posted online: 03 Oct 2013.Published online: 15 Nov 2013.

To cite this article: Hai-Tao Xia, Yu-Fen Liu & Wei-Xing Ma (2013) Study on interaction of N,N′-(2-hydroxy-3-methoxybenzyl) diamine cerium(IV) with bovine serum albumin, Journal of Coordination Chemistry, 66:21, 3706-3721, DOI: 10.1080/00958972.2013.850496

To link to this article: http://dx.doi.org/10.1080/00958972.2013.850496

Journal of Coordination Chemistry, 2013
Vol. 66, No. 21, 3706–3721, http://dx.doi.org/10.1080/00958972.2013.850496

Study on interaction of *N*,*N*′-(2-hydroxy-3-methoxybenzyl) diamine cerium(IV) with bovine serum albumin

HAI-TAO XIA*, YU-FEN LIU and WEI-XING MA

School of Chemical Engineering, Huaihai Institute of Technology, Lianyungang, China

(*Received 11 June 2013; accepted 30 August 2013*)

Complexes of cerium(IV) with bis(*N*,*N*′-(2-hydroxy-3-methoxybenzyl) ethane-1,2-diamine, bis (2-hydroxy-3-methoxybenzyl) propane-1,2-diamine and bis(2-hydroxy-3-methoxybenzyl) propane-1,3-diamine were synthesized by reaction of cerium(IV) nitrate and the ligands. The obtained coordination compounds have also been characterized by elemental analysis, IR spectroscopy, and single crystal X-ray diffraction. The interactions of these complexes with bovine serum albumin (BSA) were investigated using fluorescence spectroscopy under the simulated physiological conditions. Fluorescence titration revealed that the complexes can quench the intrinsic fluorescence of BSA through static quenching mechanism. The static quenching constants, the binding constants, and the binding sites were also acquired according to the Stern–Volmer equation and the corresponding thermodynamic parameters ΔH, ΔS, and ΔG were calculated through the van't Hoff equation. Hydrogen bonds and van der Waals forces were the predominant intermolecular forces between these complexes and BSA. The distances between BSA and these complexes were less than 8 nm, indicating that energy transfer between the donor and acceptor occurs with high probability. Synchronous fluorescence studies indicate that binding of these complexes with BSA changes the polarity around tyrosine residues rather than tryptophan residues.

Keywords: Ce(IV) complex; Crystal structure; Bovine serum albumin; Fluorescence spectrum

1. Introduction

Lanthanides have many biochemical and pharmacological actions. Lanthanide coordination chemistry is challenging due to their unique structures and their chemical, industrial, biochemical, and medicinal applications [1, 2]. Cerium is the most abundant and most widely used lanthanide metal. It has an important effect on the growth and function of blood, central nerve and immune systems, hair, skin, bone, cerebrum, liver, heart, etc. [3, 4]. Cerium is widely used in various fields of chemical engineering, luminescence, catalysis, nuclear energy, metallurgy microelectronics, therapeutic application, magnetism, etc. [5]. Ce(III/IV) complexes have been applied as versatile oxidative reagents in organic synthesis, photocatalytic oxidation, electrochemistry, and biochemistry [6]; the ligands are mainly O, N species [7–11]. *o*-Vanillin is an important raw material widely used in biology, pharmacology, catalysis, organic synthesis, chemical industry, analysis, etc. *o*-Vanillin diamine derivatives are interesting ligands that possess conformational nonrigidity, multifunction, and potential tetradentate donation (O/N) and are analogous to the biological

*Corresponding author. Email: xht161006@hhit.edu.cn

environment to some extent. Hence, *o*-vanillin is an optimal candidate for synthesizing Ce (IV) complexes with important bioactivities. Some studies indicate that incorporation of biological molecules, such as proteins and drugs, has the potential to enhance biological activities [12]. Serum albumins are the most abundant proteins in the circulatory system, playing an important role for transport, distribution, and deposition of a variety of endogenous and exogenous substances [13–15]. Various drugs injected into the body are combined with serum albumin; through the storage and transport of the plasma, they reach the receptor site to produce pharmacological effects. Many researches focus on synthesis of lanthanide complexes; however, research on the interaction mechanisms between serum albumins and lanthanides has lagged compared with research on the synthesis of lanthanide complexes, restricting the development of new types of lanthanide complexes possessing higher biological activity. Hence, it was important to investigate the interaction mechanisms between lanthanide elements and plasma proteins. In the present study, the synthesis and characterization of Ce(IV) complexes with *o*-vanillin diamine derivatives have been described. The binding properties between the Ce(IV) complexes and bovine serum albumin (BSA) were studied by fluorescence spectroscopy. The binding constants, the number of binding sites, and thermodynamic parameters between BSA and the Ce(IV) complexes are calculated at different temperatures; the interactions and binding average distance between BSA and the Ce(IV) complexes are discussed.

2. Experimental

2.1. *Materials*

BSA was purchased from the Beijing Biosea Biotechnology Company; its molecular weight is 67,000. All BSA solutions are prepared in pH 7.4 buffer solution, and BSA stock solution (1.0×10^{-4} M L^{-1}) is kept in the dark at 4 °C; NaCl (analytical grade, 0.5 M L^{-1}) is used to maintain the ion strength. Buffer solution consisted of Tris (0.05 M L^{-1}) and HCl (0.05 M L^{-1}), and the pH is adjusted to 7.4 by adding 0.1 M L^{-1} NaOH at 298 K. The Ce(IV) complex solutions (3.0×10^{-5} M L^{-1}) were prepared in ethanol. All other materials were of analytical reagent grade. All solutions are prepared with doubly-distilled water.

2.2. *Physical measurements*

Elemental analyses were measured by a Perkin–Elmer 2400c Element analyzer. Infrared spectra were recorded on a Nicolet 5DX FT-IR spectrophotometer using KBr disks from 4000 to 400 cm^{-1}. Fluorescence spectra were measured with a Shimadzu RF-5301 fluorophotometer equipped with a 150 W Xenon lamp and 1.0 cm quartz cell. Absorption spectra were obtained by a Shimadzu UV-2550 PC spectrophotometer.

2.3. *Preparation of complexes*

The preparation of ligands follows the procedure in the literature [16, 17]. Cerium(IV) complexes were obtained according to the following general procedure: $Ce(NO_3)_3 \cdot 6H_2O$ (5 mM) was dissolved in 10 mL ethanol, followed by addition of the ligand L_1 (bis (*N*,*N*′-(2-hydroxy-3-methoxybenzyl) ethane-1,2-diamine, 10 mM) or L_2 (bis(2-hydroxy-3-methoxybenzyl) propane-1,2-diamine, 10 mM) or L_3 (bis(2-hydroxy-3-methoxybenzyl)

propane-1,3-diamine, 10 mM). The reaction mixture was stirred in air for 3–4 h and then filtered. Crystals of $[Ce(L_1)_2]$ and $[Ce(L_2)_2]$ suitable for crystallographic characterization and solids of $[Ce(L_3)_2]$ were obtained by evaporation of an ethanol solution. The synthetic pathway for the complexes may be represented by scheme 1. Results of elemental analyses:

Anal. Calcd for $[Ce(L_1)_2]$ (**1**) $[C_{36}H_{44}N_4O_8Ce]$ (%): C, 53.99; H, 5.54; N, 7.00. Found (%): C, 53.86; H, 5.49; N, 6.92. IR (KBr, $\nu(cm^{-1})$): 3256, 2944, 2854, 1590, 1479, 1443, 1308, 1278, 1239, 1077, 927, 840, 735.

Anal. Calcd for $[Ce(L_2)_2]$ (**2**) $[C_{38}H_{48}N_4O_8Ce]$ (%): C, 55.06; H, 5.84; N, 6.76. Found (%): C, 54.91; H, 5.77; N, 6.63. IR (KBr, $\nu(cm^{-1})$): 3250, 2944, 2842, 1593, 1476, 1380, 1275, 1233, 1074, 978, 843, 729.

Anal. Calcd for $[Ce(L_3)_2]$ (**3**) $[C_{38}H_{48}N_4O_8Ce]$ (%): C, 55.06; H, 5.84; N, 6.76. Found (%): C, 54.95; H, 5.73; N, 6.68. IR (KBr, $\nu(cm^{-1})$): 3406, 2944, 2854, 1596, 1548, 1422, 1383, 1236, 1071, 957, 840, 732.

2.4. *Crystal structure determination*

Dark red crystals of $[Ce(L_1)_2]$ (**1**) crystallized in the monoclinic space group $P2_1/c$, whereas dark red crystals of $[Ce(L_2)_2]$ (**2**) crystallized in the orthorhombic space group P_{bca}. Diffraction data were collected with a Bruker SMART 1000 CCD diffractometer by the use of graphite monochromated Mo Kα radiation (λ = 0.71073 Å) at 298(2) K. The crystal structure was solved by direct methods and all nonhydrogen atoms were located with successive difference Fourier syntheses. The structure was refined by full-matrix least squares on F^2 with anisotropic thermal parameters for all nonhydrogen atoms. The hydrogens were added according to theoretical models. All calculations were performed using the programs in SHELXL [18, 19].

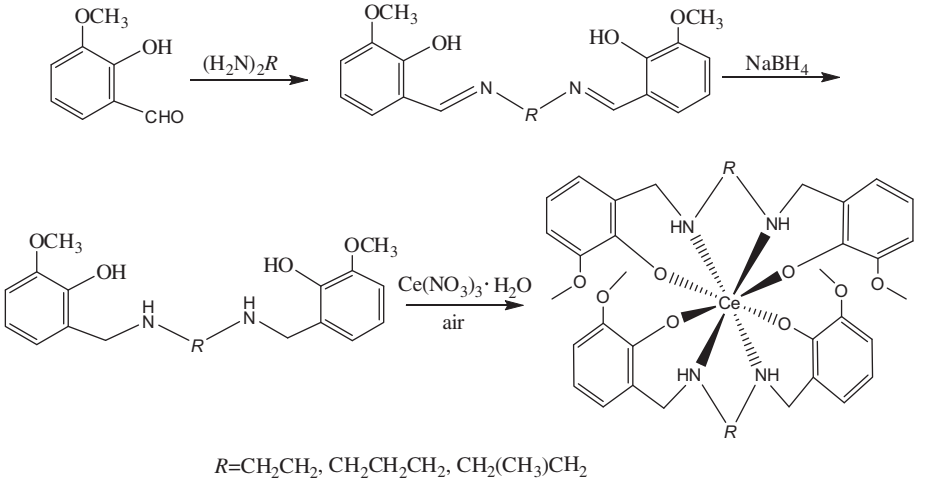

R=CH_2CH_2, $CH_2CH_2CH_2$, $CH_2(CH_3)CH_2$

Scheme 1. The synthetic pathway for the cerium(IV) complexes.

2.5. *Fluorescence spectra*

The fluorescence measurements of complex-BSA solutions are performed at different temperatures by keeping the concentration of BSA fixed at 4×10^{-6} M L^{-1} while varying the Ce(IV) complex concentration from 0 to 10×10^{-6} M L^{-1}. The widths of both the excitation slit and the emission slit are set to 10 and 5.0 nm. Fluorescence spectra were recorded from 300 to 500 nm at an excitation wavelength of 285 nm.

2.6. *Energy transfer*

The absorption spectra of Ce(IV) complexes were recorded at 298 K from 300 to 500 nm. The emission spectrum of BSA was also recorded at 298 K in the same range. Then, the overlap of the UV absorption spectrum of Ce(IV) complexes with the fluorescence emission spectrum of BSA wase used to calculate the energy transfer.

2.7. *Synchronous fluorescence spectra*

The synchronous fluorescence spectra were collected with $\Delta\lambda = 15$ and $\Delta\lambda = 60$ nm, respectively, in the same experimental conditions.

3. Results and discussion

3.1. *Crystal structure description*

Details of the diffraction experiment, structure refinement, and selected bond distances and angles for [Ce(L$_1$)$_2$] (**1**) are presented in tables 1 and 2. The crystal structure of **1** has been reported [20]. Complex **2** is formed by complexation of Ce(IV) with two ligands. Each

Table 1. Crystal data and structure refinement for **1** and **2**.

Formula	$C_{36}H_{44}N_4O_8Ce$ (**1**)	$C_{38}H_{48}N_4O_8Ce$ (**2**)
Formula weight	800.87	828.92
Temperature (K)	298(2)	298(2)
Wavelength (Å)	0.71073	0.71073
Crystal system	Monoclinic	Orthorhombic
Space group	$P2_1/c$	P_{bca}
Unit cells and dimensions (Å, °)		
a	23.166(3)	11.4384(16)
b	17.803(2)	14.1272(18)
c	27.883(4)	46.433(3)
α	90	90
β	110.116(3)	90
γ	90	90
Volume (Å^3), Z	10,798(2), 12	7503.3(15), 8
Calculated density (Mg m^{-3})	1.478	1.468
F (0 0 0)	4920	3408
Crystal size (mm^3)	0.39 × 0.35 × 0.32	0.44 × 0.28 × 0.12
θ Range for data collection (°)	1.38 – 25.01	1.98 – 25.01
Reflections collected	53,789	30,706
Independent reflection	18,893 [R(int) = 0.0868]	6182 [R(int) = 0.1287]
Refinement method	Full-matrix least-squares on F^2	Full-matrix least-squares on F^2
Data/restraints/parameters	18,893/48/1328	6182/0/466
Goodness-of-fit on F^2	0.936	1.029
Final R indices [$I > 2\sigma(I)$]	$R_1 = 0.0409$, $wR_2 = 0.0680$	$R_1 = 0.0994$, $wR_2 = 0.1857$
Largest diff. peak and hole (eÅ^{-3})	1.404 and −1.021	2.073 and −2.325

Table 2. The selected bond lengths (Å), hydrogen bond lengths (Å), and bond angles (°) for **2**.

Ce1–O3	2.200(10)	Ce1–N3	2.586(14)	
Ce1–O5	2.205(11)	Ce1–N2	2.598(13)	
Ce1–O7	2.220(10)	Ce1–N4	2.604(13)	
Ce1–O1	2.224(10)	Ce1–N1	2.605(13)	
O3–Ce1–O5	90.4(4)	N3–Ce1–N2	130.7(5)	
O3–Ce1–O7	96.6(4)	O3–Ce1–N4	81.9(4)	
O5–Ce1–O7	149.0(4)	O5–Ce1–N4	138.1(5)	
O3–Ce1–O1	150.3(12)	O7–Ce1–N4	72.9(4)	
O5–Ce1–O1	97.0(4)	O1–Ce1–N4	73.3(4)	
O7–Ce1–O1	91.7(4)	N3–Ce1–N4	66.6(5)	
O3–Ce1–N3	74.2(4)	N2–Ce1–N4	139.9(4)	
O5–Ce1–N3	71.6(5)	O3–Ce1–N1	138.8(4)	
O7–Ce1–N3	139.3(4)	O5–Ce1–N1	81.9(4)	
O1–Ce1–N3	80.9(4)	O7–Ce1–N1	72.9(4)	
O3–Ce1–N2	72.4(4)	O1–Ce1–N1	70.9(4)	
O5–Ce1–N2	73.5(4)	N3–Ce1–N1	138.4(4)	
O7–Ce1–N2	79.9(4)	N2–Ce1–N1	66.6(4)	
O1–Ce1–N2	137.3(4)	N4–Ce1–N1	128.9(5)	
D–H···*A*	*D*–H	H···*A*	D···*A*	∠ *D*–H···*A*
N1–H1···O8	0.91	2.29	3.188(17)	169
N2–H2···O6	0.91	2.65	3.530(18)	162
N3–H3···O4	0.91	2.26	3.148(18)	166
N4–H4···O2	0.91	2.47	3.358(18)	167
C4–H4A···O7^{i}	0.97	2.69	3.332(18)	125

Symmetry codes: (i) $-x + 1/2, y + 1/2, z$.

ligand forms four coordinate bonds to the central ion (figure 1). The Ce–O and Ce–N distances vary between 2.200(10) and 2.224(10) Å and between 2.586(14) and 2.605(13) Å, respectively. The Ce–O distances for **2** are longer than for **1** and are similar to those observed for $[CeC_{40}H_{40}N_4O_4]$ (2.148(7)–2.241(9) Å) [21]. The Ce–N bond lengths are shorter than those found for **1** and are similar to $CeC_{40}H_{40}N_4O_4$ [21] of (2.525(11)–2.619 (9) Å). The shorter Ce–N distances indicated that the coordination of N are strengthened owing to the repulsive electron effect of methyl, and elongations of Ce–O bonds are a result of shortened Ce–N bonds.

The angles formed by the same donors are similar for both ligands. The O–Ce–O angles are the largest, 149.0(4) and 150.3(4)° for O5–Ce1–O7 and O3–Ce1–O4, respectively. The angles formed by the adjacent oxygens of different ligands are approximately vertical, varying between 90.4(4) and 91.7(4)°, and are similar to those of 90.74(14) and 90.12(13)° observed in **1**. Due to two ligands in the sphere, the angles between the coordination bonds formed by different ligands vary from 72.9(4)° for O7–Ce1–N1 to 139.9(4)° for N2–Ce1–N4.

The dihedral angles between phenyl ring planes are 42.1(4)° for C1–C19 and 38.2(4)° for C20–C38. The dihedral angles between adjacent phenyl rings of different ligands are 19.0(6)° for C5–C10 and C32–C37 rings, and 19.4(5)° for C13–C18 and C24–C29 rings, while others are 48.4(4)° for C5–C10 and C24–C29 rings, and 40.9(4)° for C13–C18 and C32–C37 rings. The dihedral angle between CeN_2O_2 coordination planes formed by the two ligands is 84.4(2)°. The dihedral angles between the CeN_2O_2 coordination plane and the ring planes are 35.1(5) and 40.6(4)° for C5–C10 and C13–C18 rings for the first ligand, and 33.7(5) and 39.3(4)° for C24–C29 and C32–C37 rings of the second ligand.

Molecules of **2** are linked into chains by C–H···O intermolecular hydrogen bonds (table 2). There are direction-specific interactions between adjacent chains in the 3-D network structure.

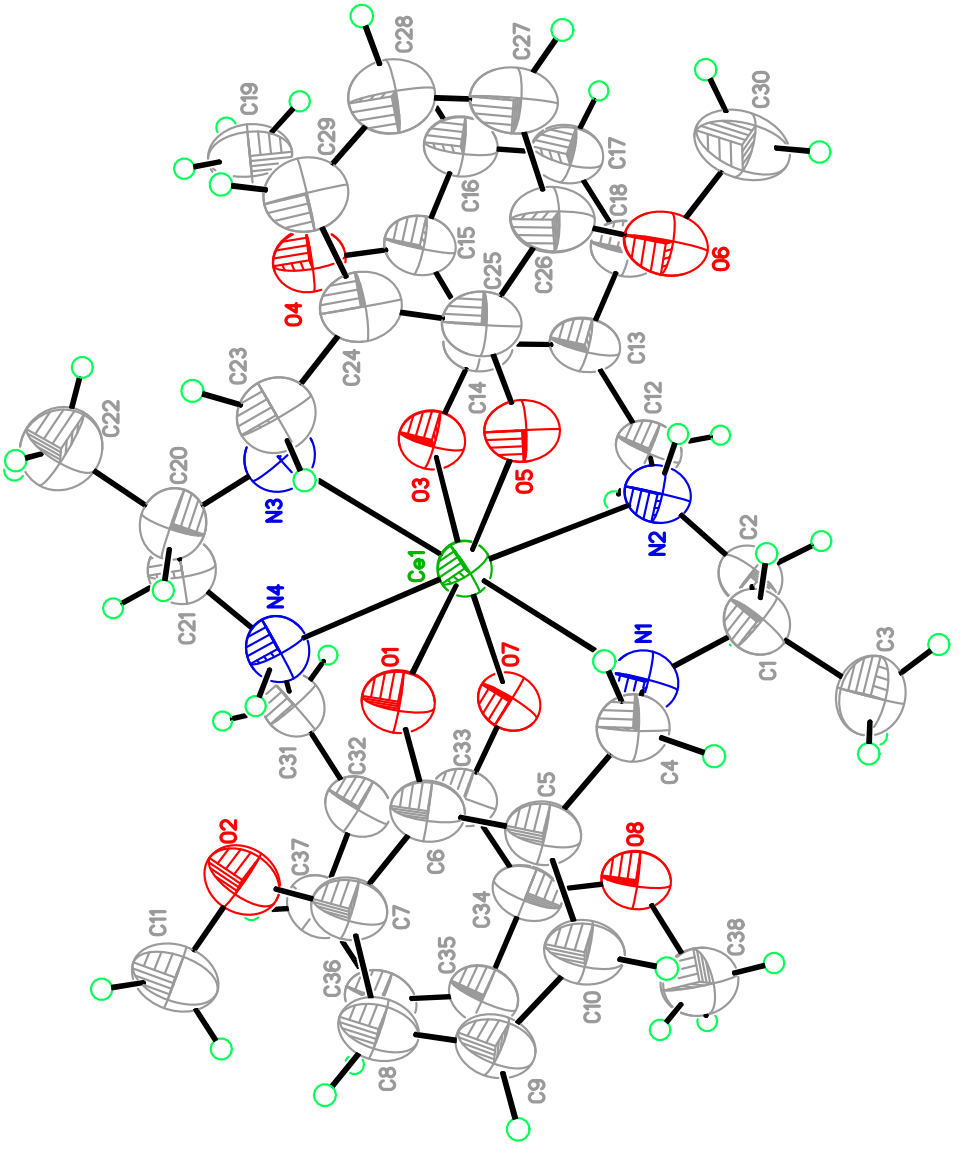

Figure 1. Molecular structure of **2**.

3.2. *Fluorescence spectroscopy*

Interactions of **1**, **2**, and **3** with BSA have been studied from tryptophan emission quenching experiments. BSA contains three fluorophores, tryptophan, tyrosine, and phenylalanine; the intrinsic fluorescence of BSA is mainly contributed by tryptophan. BSA has two tryptophan residues along the chain. Trp-134 is located on the surface of the protein and Trp-212 is located within a hydrophobic binding pocket of the protein. The tryptophan residues can bind reversibly to a large number of exogenous and endogenous compounds. The change in the emission spectra of tryptophan is primarily due to protein conformation transitions,

subunit association, substrate binding, or denaturation [22]. Figure 2 shows the fluorescence emission spectra of BSA in the absence and presence of the complexes. BSA exhibits a strong fluorescence emission at 346 nm due to tryptophan residues when excited at 285 nm. When a different concentration of the complexes solution was titrated into a fixed concentration of BSA, a decrease in the fluorescence intensity of BSA was observed, indicating that there were interactions and energy transfer between the complexes and BSA.

Fluorescence quenching refers to the decrease in the fluorescence intensity of a fluorophore induced by molecular interactions with quencher molecule. The mechanism of the quenching may be either through static or dynamic quenching. Static quenching refers to quenching through fluorophore–quencher complex formation and dynamic quenching refers to a process where the fluorophore and the quencher come into contact during the transient existence of the excited state. Fluorescence quenching can be analyzed by using the Stern-Volmer equation [23]:

$$F^0/F = 1 + K_q\tau_0[Q] = 1 + K_{sv}[Q]$$

where F^0 and F represent the fluorescence intensities of BSA solution at 346 nm in the absence and presence of quencher, respectively. K_q is the quenching rate constant, K_{sv} is the dynamic quenching constant, τ_0 is the average lifetime of the biomolecule without quencher and taking as fluorescence lifetime of tryptophan in BSA at around 10^{-8} s, and [Q] is the concentration of quencher. Figure 3 displays the Stern-Volmer plots of the quenching of BSA fluorescence by complexes at different temperatures. The Stern-Volmer quenching constant K_{sv} can be obtained by the slope of the diagram F^0/F versus $[Q]$, and subsequently the approximate quenching constant K_q may be calculated. Quenching mechanism can be predicted from Stern-Volmer plots. As shown in figure 4, the plot exhibited a good linear relationship, suggesting that a single quenching mechanism, either static or dynamic, occurs at the experiment concentrations [24]. The upper limit of K_q expected for a diffusion-controlled bimolecular process is 2.0×10^{10} M L^{-1} s^{-1} [25]; the high magnitude of all the K_q values in the present study (10^{12} L M^{-1} s^{-1}, table 3) indicates that fluorescence quenching effects of complexes are not initiated by dynamic collision but by formation of the complex.

3.3. *Binding constants and the number of binding sites*

For static quenching, the binding constant and the number of binding sites can be determined by the following equation [23]:

$$\log[(F^0 - F)/F] = \log K_b + n\log[Q]$$

where K_b and n are the binding constant and the number of binding sites, respectively. According to the equation, binding parameters can be obtained by a plot of the double-logarithm curve log $[(F^0 - F)/F]$ versus log $[Q]$ (figure 4). The values of K_b and n were calculated from the values of intercept and slope of the plots, respectively; the corresponding results are summarized in table 3. The binding constants decreased with increasing temperature, indicating that stability of the complex-BSA system is reduced. They are probably associated with hydrogen bonding and weakening of the complex-BSA stability. The values of n at the experimental temperatures were approximately equal to 1, indicating that there is one class of binding site on BSA for **1**, **2**, and **3**. The values of K_b indicate that there is a

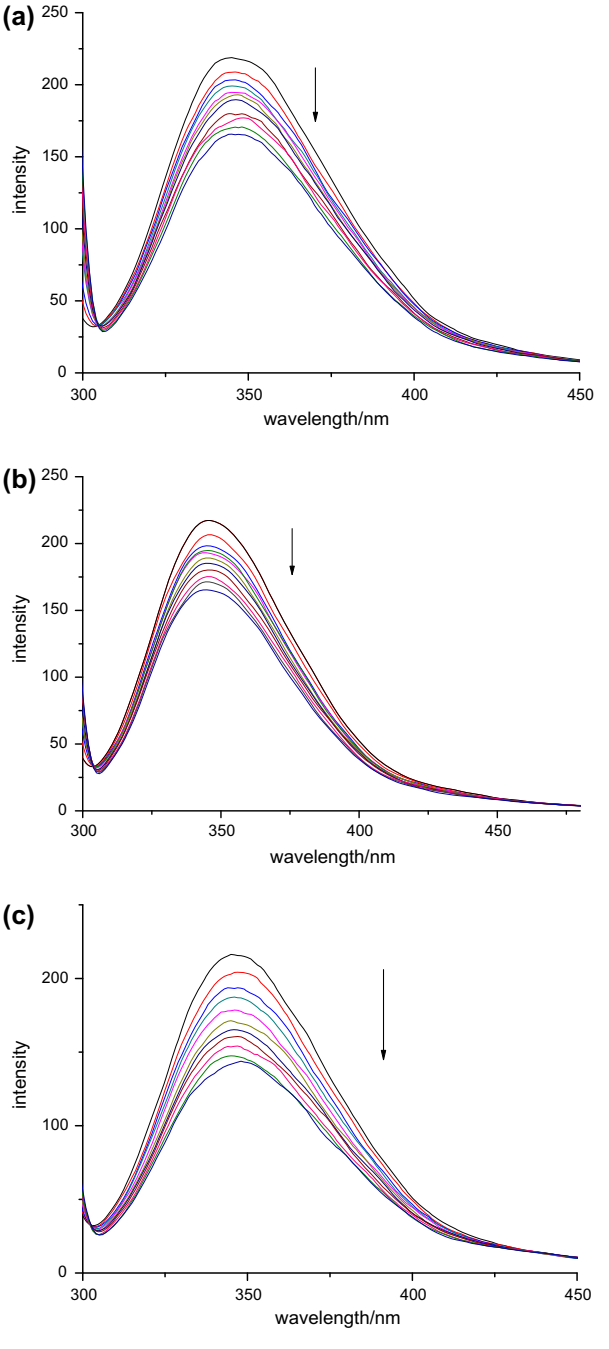

Figure 2. Emission spectra of BSA in the presence and absence of **1**, **2** and **3**. [BSA]: 4×10^{-6} M L^{-1}; [complex]: 0, 1, 2, 3, 4, 5, 6, 7, 8, 9, 10×10^{6} M L^{-1}. λ_{ex} = 285 nm; λ_{em} = 346 nm; pH = 7.4; T = 298 K.

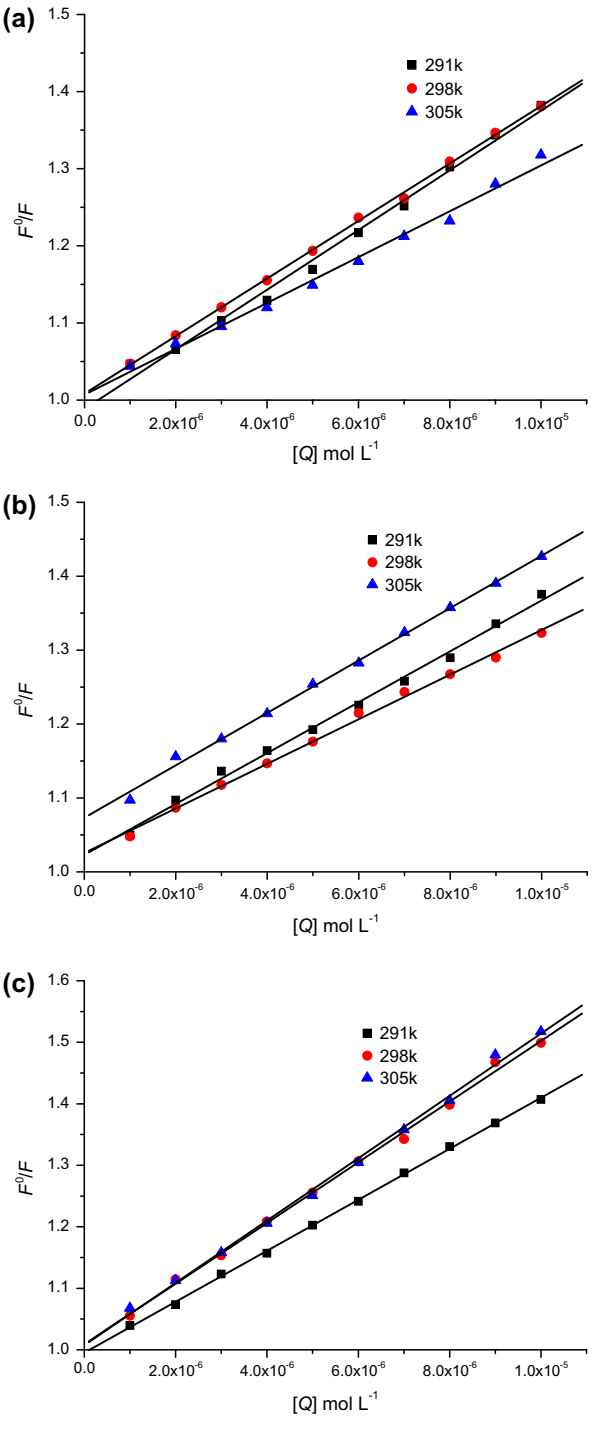

Figure 3. The Stern-Volmer plots for the interaction of complexes with BSA.

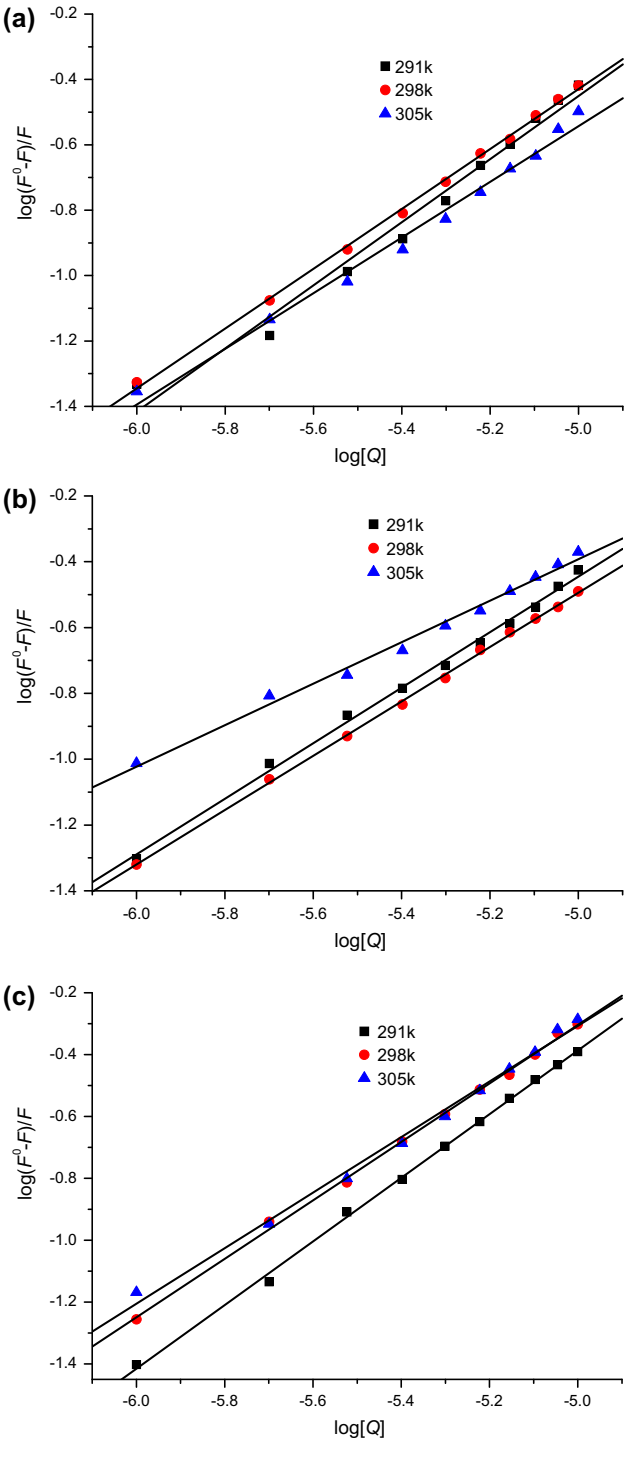

Figure 4. Plots of $\log(F^0 - F)/F$ *vs.* $\log[Q]$.

Table 3. Binding constants and thermodynamic parameters.

Complex	T (K)	K_{sv} ($L\,M^{-1}$)	K_q ($L\,M^{-1}\,s^{-1}$)	K_b ($L\,M^{-1}$)	n	ΔH ($kJ\,M^{-1}$)	ΔG ($kJ\,M^{-1}$)	ΔS ($J\,M^{-1}\,K^{-1}$)
1	291	3.87×10^4	3.87×10^{12}	2.39×10^4	0.97	−80.27	−24.61	−191.18
	298	3.73×10^4	3.72×10^{12}	1.42×10^4	0.92		−23.27	
	305	2.97×10^4	2.97×10^{12}	5.19×10^3	0.85		−21.93	
2	291	3.44×10^4	3.44×10^{12}	5.97×10^3	0.84	−122.56	−21.73	−346.31
	298	3.02×10^4	3.02×10^{12}	4.32×10^3	0.83		−19.31	
	305	3.55×10^4	3.55×10^{12}	5.77×10^2	0.63		−16.88	
3	291	4.15×10^4	4.15×10^{12}	5.72×10^4	1.03	−69.72	−26.44	−148.65
	298	4.93×10^4	4.93×10^{12}	2.66×10^4	0.95		−25.40	
	305	5.07×10^4	5.07×10^{12}	1.53×10^4	0.90		−24.36	

moderate interaction between complexes and BSA. The binding propensity of **3** was higher than **1** and **2**.

Compared with studies dealing with copper complexes-BSA interaction [23, 26, 27], few studies on cerium complexes have been reported. Comparing K_b and n values of **1**, **2**, and **3** with those of copper complexes, including analogous ligands, we find that the K_b and n values of the copper complexes $[Cu_2(oxbpa)(phen)(H_2O)](pic)\cdot 2H_2O$ (K_b, $2.09 \times 10^6\,L\,M^{-1}$; n, 1.23) [26] and $[C_{20}H_{32}Cu_2I_3N_4]_n$ (K_b, $5.95 \times 10^8\,L\,M^{-1}$; n, 1.68) [23] are both higher, implying that interactions of this class of complexes toward BSA depend on the nature of metal ions and ligands; medicinal properties of complexes may be tuned by changing the metal ions or ligands.

3.4. *Binding mode*

The interaction between any drug and biomolecule include hydrogen bonds, van der Waals forces, electrostatic forces, and hydrophobic interaction. These forces can be identified from studies on thermodynamics of binding of drug molecules with proteins. In order to elucidate the interaction between the complexes and BSA, the thermodynamic parameters were calculated on the basis of the van't Hoff equation [23]. The thermodynamic parameters for the interaction of the complexes with BSA are shown in table 3. The negative values of ΔG indicate that the binding process is spontaneous. According to the rules summarized by Ross and Subramanian [28], negative values of enthalpy (ΔH) and entropy (ΔS) indicate that the hydrogen bonds and van der Waals forces played a major role in the binding of **1**, **2**, and **3** with BSA.

3.5. *Synchronous fluorescence*

Synchronous fluorescence spectra of BSA can be used to detect the change in conformation of BSA. When $\Delta\lambda$ between excitation wavelength and emission wavelength is fixed at 15 or 60 nm, synchronous fluorescence can provide information on the environment of tyrosine and tryptophan residues in BSA [29]. The synchronous fluorescence spectra of BSA in the presence of the complexes are shown in figure 5. The maximum emission wavelength of tyrosine residue shows an obvious red shift in the presence of **1**, **2**, and **3**, suggesting that the polarity around the tyrosine residues decreased. In contrast, no significant shift was observed when $\Delta\lambda$ = 60 nm suggesting that interaction of the complexes with BSA does not affect the polarity and conformation of the tryptophan residue micro-region.

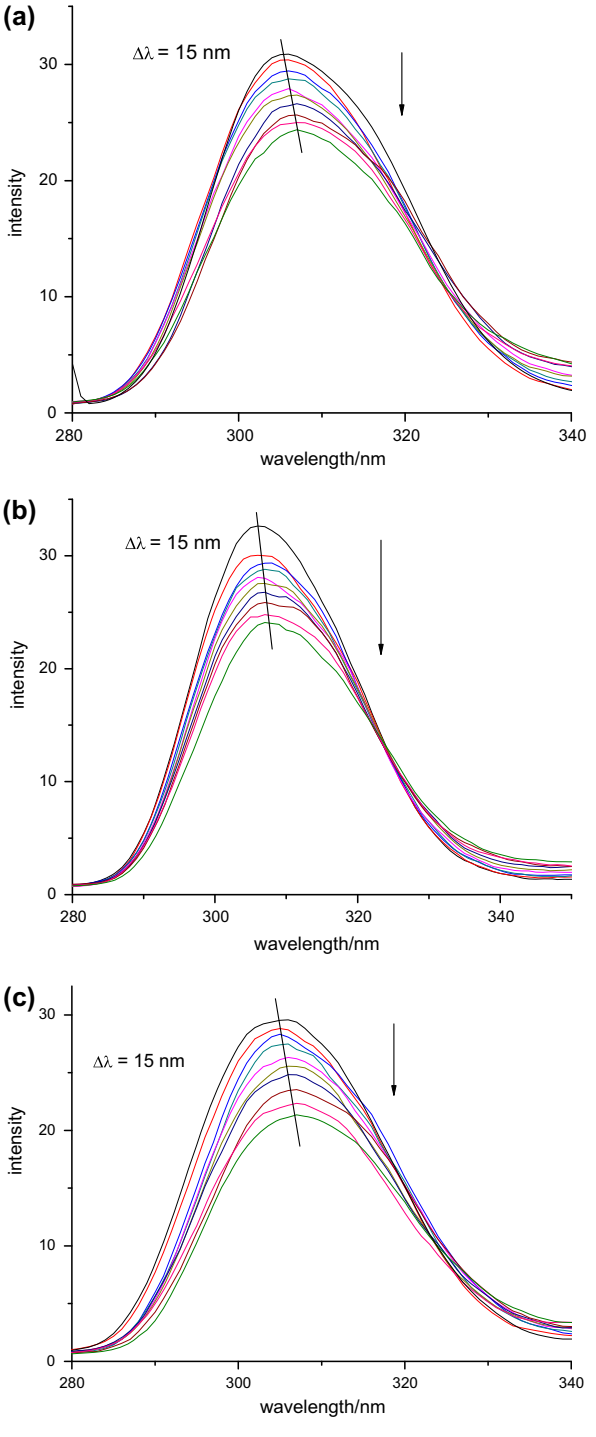

Figure 5. Synchronous fluorescence spectra of interaction between BSA and complexes. [BSA]: 4×10^{6} M L^{-1}; [complex]: 0, 1, 2, 3, 4, 5, 6, 7, 8, 9×10^{-6} M L^{-1}; pH = 7.4; T = 298 K.

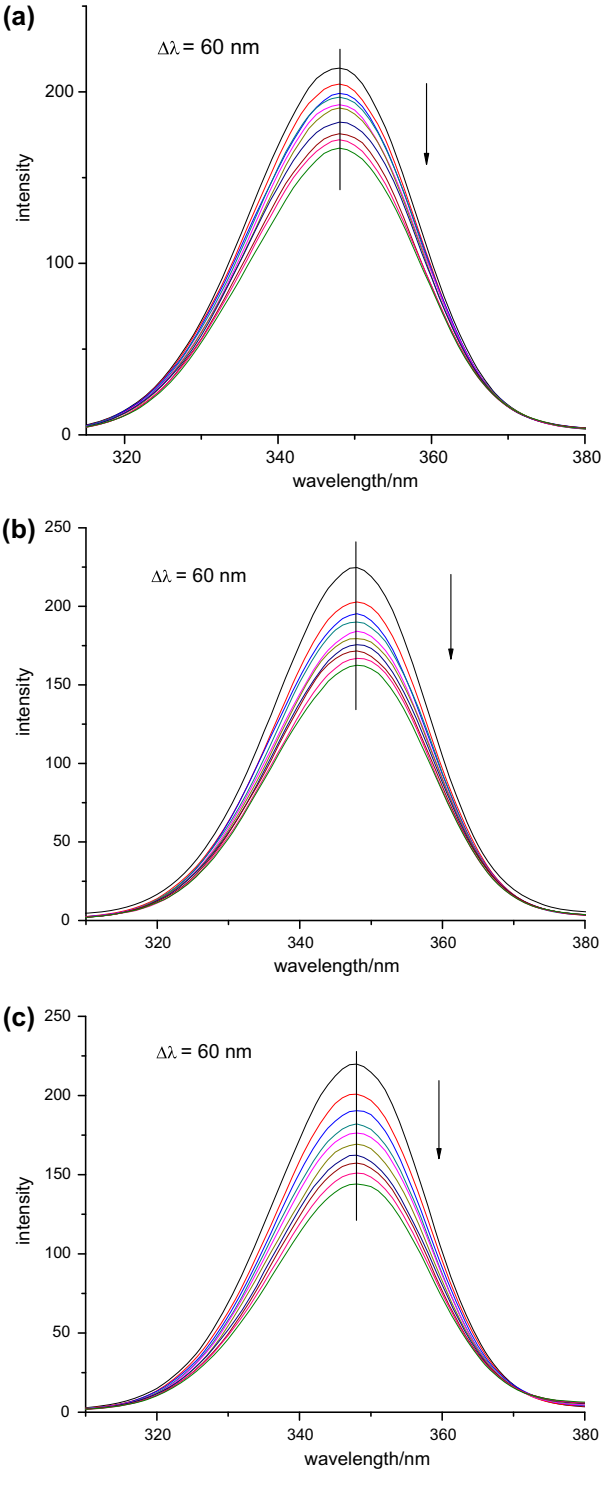

Figure 5. (*Continued*).

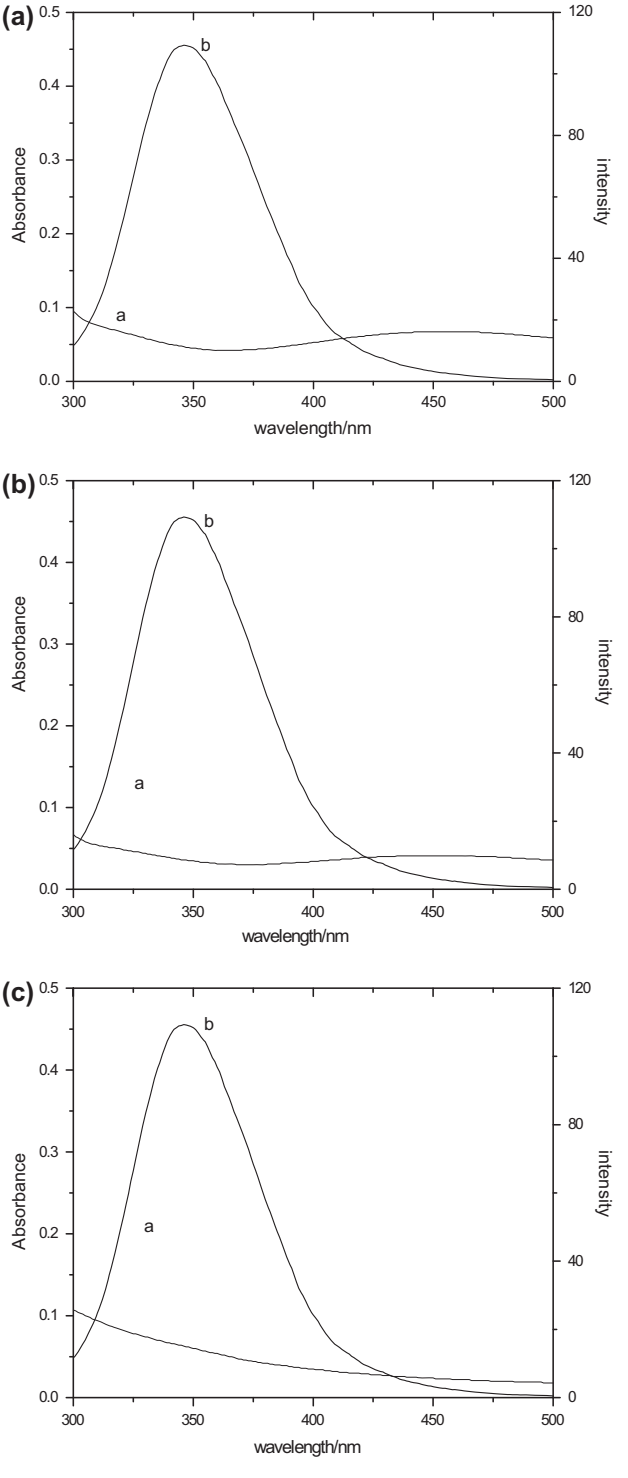

Figure 6. Spectral overlap of complexes absorption (a) with BSA fluorescence (b) [BSA] = [complexes]: 1×10^5 M L^{-1} (T = 291 K).

Table 4. Relevant parameters of complexes-BSA systems.

Complex	J (cm^3 L M^{-1})	E (%)	R_0 (nm)	r (nm)
1	8.58×10^{15}	0.12	4.38	6.11
2	6.09×10^{15}	0.14	4.13	5.59
3	8.90×10^{15}	0.13	4.40	6.04

3.6. *Energy transfer between the complexes and BSA*

The fluorescence quenching of BSA in the presence of complexes indicated that energy transfer between **1**, **2**, **3**, and BSA occurred. According to Förster nonradiative energy transfer theory, the energy transfer efficiency is described by the following equation:

$$E = 1/[1 + (r/R_0)^6] = 1 - (F/F^0)$$

where E is the efficiency of energy transfer between the donor and acceptor, F and F^0 are the fluorescence intensities of BSA in the presence and absence of the complexes, r is the distance between the donor and acceptor, and R_0 is the critical distance at which transfer efficiency equals 50%. The value of R_0 can be calculated using the following equation:

$$R_0^6 = 8.79 \times 10^{-25}(K^2 \cdot N^{-4} \cdot \Phi \cdot J)$$

where K^2 is the spatial orientation factor of the dipole, N is refractive index of the medium, Φ is fluorescence quantum yield of the donor, and J is overlap integral of the fluorescence emission spectrum of donor and absorption spectrum of the acceptor. The UV–Vis absorption spectrum of the complexes with the fluorescence emission spectrum of BSA is shown in figure 6. J can be calculated by the following equation:

$$J = \frac{\int_0^\infty F(\lambda)\varepsilon(\lambda)\lambda^4 \mathrm{d}\lambda}{\int_0^\infty F(\lambda)\mathrm{d}\lambda}$$

where $F(\lambda)$ is the fluorescence intensity of the donor in the wavelength range λ–$\lambda + \Delta\lambda$ and $\varepsilon(\lambda)$ is the molar absorption coefficient of the acceptor at wavelength λ. In the present case, $K^2 = 2/3$, $N = 1.336$, $\Phi = 0.15$ [23]. From the overlapping spectrum, J can be evaluated by integrating the spectra for λ = 300–500 nm; the corresponding results are summarized in table 4. Obviously, the distance between the donor BSA and the acceptor (complex) is less than 8 nm, and $0.5\ R_0 < r < 1.5\ R_0$, indicating that the binding of **1**, **2**, and **3** with BSA occurs through energy transfer.

4. Conclusions

Three eight-coordinate Ce(IV) complexes with *N*,*N*′-(2-hydroxy-3-methoxybenzyl) diamine were synthesized and the crystal structures of **1** and **2** were determined by single crystal X-ray diffraction. The interactions of the complexes with BSA in physiological buffer solution were studied by fluorescence spectroscopic methods. Decreasing values of binding constants of **1**, **2**, and **3** with increasing temperature indicated interaction with BSA through a static quenching procedure. The values of n revealed the presence of one binding site on BSA. The thermodynamic parameters of the binding interaction were determined and their

values suggested that hydrogen bonds and van der Waals forces played major roles in the interactions of Ce(IV) complexes (**1**, **2**, and **3**) with BSA. The binding distances *r* between Ce(IV) complexes and BSA indicate that energy transfer from BSA to Ce(IV) complexes occurs. The synchronous fluorescence spectroscopy indicates that the conformation of BSA changed in the presence of Ce(IV) complexes.

Supplementary material

Crystallographic data for the structures in this article have been deposited with the Cambridge Crystallographic Data Center as supplementary publication CCDC Nos. 635372 and 653349 for **1** and **2**. Copies of the data can be obtained, free of charge, on application to CCDC, 12 Union Road, Cambridge CB2 1EZ, UK.

References

[1] O.-S. Jung, S.-H. Park, Y.-A. Lee, D.-C. Kim. *J. Mol. Struct.*, **645**, 281 (2003).
[2] I. Kostova, I. Manolov, G. Momekov, T. Tzanova, S. Konstantinov, M. Karaivanova. *Eur. J. Med. Chem.*, **40**, 1246 (2005).
[3] J.-M. Li, W.-T. Wei. *J. Rare Earth*, **28**, 387 (2010).
[4] M.Y. Khotimchenko, E.A. Kolenchenko, Y.S. Khotimchenko, E.V. Khozhaenko, V.V. Kovalevb. *Colloids Surf., B*, **77**, 104 (2010).
[5] Z.V.P. Murthy, A. Choudhary. *Desalination*, **279**, 428 (2011).
[6] L. Li, F. Yuan, T.-T. Li, Y. Zhou, M.-M. Zhang. *Inorg. Chim. Acta*, **397**, 69 (2013).
[7] I. Kostova, G. Momekov. *Eur. J. Med. Chem.*, **43**, 178 (2008).
[8] M.R. Ganjali, M. Hosseini, Z. Memari, F. Faridbod, M. Hakimi, E. Motieiyan, A. Shokrollahi, A.N. Haghighi. *Inorg. Chim. Acta*, **385**, 140 (2012).
[9] C.M. Kizas, C. Papatriantafyllopoulou, M.J. Manos, A.J. Tasiopoulos. *Polyhedron*, **52**, 346 (2013).
[10] Nibha, I.P.S. Kapoor, G. Singh, R. Fröhlich. *J. Mol. Struct.*, **1034**, 296 (2013).
[11] T.V. Balashova, A.P. Pushkarev, V.A. Ilichev, M.A. Lopatin, M.A. Katkova, E.V. Baranov, G.K. Fukin, M.N. Bochkarev. *Polyhedron*, **50**, 112 (2013).
[12] S.R.S. Ting, J.M. Whitelock, R. Tomic, C. Gunawan, W.Y. Teoh, R. Amal, M.S. Lord. *Biomaterials*, **344**, 377 (2013).
[13] N. Shahabadi, M. Maghsudi. *J. Mol. Struct.*, **929**, 193 (2009).
[14] J.-N. Tian, J.-Q. Liu, Z.-D. Hu. *Bioorg. Med. Chem.*, **13**, 4124 (2005).
[15] T.-H. Wang, Z.-M. Zhao, B.-Z. Wei, L. Zhang, L. Ji. *J. Mol. Struct.*, **970**, 128 (2010).
[16] H.-T. Xia, Y.-F. Liu, S.-P. Yang, D.-Q. Wang. *Acta Cryst.*, **E62**, o5864 (2006).
[17] H.-T. Xia, Y.-F. Liu, S.-P. Yang, D.-Q. Wang. *Acta Cryst.*, **E63**, o239 (2007).
[18] G.M. Sheldrick. *SHELXS-97, Program of X-ray Crystal Structure Solution*, University of Göttingen, Göttingen, Germany (1997).
[19] G.M. Sheldrick. *SHELXL-97, Program for X-ray Crystal Strucuture Refinement*, University of Göttingen, Göttingen, Germany (1997).
[20] Y.-F. Liu, H.-T. Xia, D.-Q. Wang, S.-P. Yang. *Acta Cryst.*, **E63**, m484 (2007).
[21] E. Szłyk, A. Wojtczak, L. Dobrzańska, M. Barwiołek. *Polyhedron*, **27**, 765 (2008).
[22] Y.-Q. Wang, H.-M. Zhang, G.-C. Zhang, W.-H. Tao, Z.-H. Fei, Z.-T. Liu. *J. Pharm. Biomed. Anal.*, **43**, 1869 (2007).
[23] Y.-F. Liu, H.-T. Xia, D.-F. Rong. *J. Coord. Chem.*, **65**, 2919 (2012).
[24] F. Xue, C.-Z. Xie, Y.-W. Zhang, Z. Qiao, X. Qiao, J.-Y. Xu, S.-P. Yan. *J. Inorg. Biochem.*, **115**, 78 (2012).
[25] N. Shahabadi, M. Maghsudi. *J. Mol. Struct.*, **929**, 193 (2009).
[26] X.-L. Wang, M. Jiang, Y.-T. Li, Z.-Y. Wu, C.-W. Yan. *J. Coord. Chem.*, **66**, 1985 (2013).
[27] Y.-F. Liu, X.-Y. Xu, H.-T. Xia, D.-Q. Wang, H. Liu. *Synth. React. Inorg. Met.-Org. Nano-Met. Chem.*, **39**, 400 (2009).
[28] P.D. Ross, S. Subramanian. *Biochemistry*, **20**, 3096 (1981).
[29] G. Vignesh, S. Arunachalam, S. Vignesh, R.A. James. *Spectrochim. Acta, Part A*, **96**, 108 (2012).